Available online at www.sciencedirect.com
SCIENCE DIRECT®
International Journal of Heat and Mass Transfer 48 (2005) 2198–2208
International Journal of HEAT and MASS TRANSFER
www.elsevier.com/locate/ijhmt

The effect of sheath on plasma momentum transport to an electrically biased surface

F.B. Yeh [a,*], P.S. Wei [b,1]

[a] Department of Marine Mechanical Engineering, Chinese Naval Academy, P.O. Box 90175, Kaohsiung, Taiwan, ROC
[b] Department of Mechanical and Electro-Mechanical Engineering, National Sun Yat-Sen University, Kaohsiung, Taiwan, ROC

Received 13 May 2004; received in revised form 31 December 2004
Available online 13 March 2005

Abstract

Ion and electron momentum fluxes transport to a biased workpiece surface in contact with a plasma are systematically and kinetically investigated in this study. Micro-electro-mechanical systems (MEMS), semiconductor technology, plasma etching, spray deposition, sputtering, cutting and surface treatment, etc. are strongly affected by momentum transfer from the plasma to workpiece. In this work, the plasma is composed of a collisionless presheath and sheath on an electrically negative biased surface that partially reflects or secondly emits ions and electrons. The presheath is an ionization region that continuously produces ions to maintain ion loss to the workpiece, while the sheath is a space-charge region that accelerates ions and retards electrons to the negative biased surface. The predicted total momentum flux at the wall including that of the ions and electrons as a function of negative electrically biased voltage is found to agree well with experimental data. The effects of the sheath and plasma parameters such as net current density, ion and electron reflectivities of the wall, ion-to-electron mass ratio, charge number, electron-to-ion source temperature ratio at the presheath edge, on the total momentum flux, ion and electron momentum fluxes, and their components through the sheath to the surface are obtained.
© 2005 Elsevier Ltd. All rights reserved.

Keywords: Plasma momentum flux; Kinetic ion and electron momentum fluxes; Sheath; Presheath; Momentum flux on a negative electrically biased surface

1. Introduction

Determination of momentum fluxes to a workpiece surface in contact with plasma is important. Micro-electro-mechanical systems (MEMS), semiconductor technology, plasma etching, spray deposition, sputtering, cutting, surface treatment of plasma processing, designing divertors and limiters in nuclear fusion, etc., are strongly affected by momentum transfer from the plasma to a surface. In contrast to momentum transfer from neutral and ordinary gases, the momentum flux from the plasma to the workpiece surface is controlled by sheath voltage in front of the surface. Since mobilities of ions and electrons are different, the plasma exhibits net positive charges with respect to the wall [1]. Debye shielding confines the negative potential to a thin layer called the sheath or space-charge region in a thickness of around

* Corresponding author. Tel./fax: +886 7 5834861.
E-mail addresses: fbyeh@mail.cna.edu.tw (F.B. Yeh), pswei@mail.nsysu.edu.tw (P.S. Wei).
[1] Fax: +886 7 5254214/5254299.

0017-9310/$ - see front matter © 2005 Elsevier Ltd. All rights reserved.
doi:10.1016/j.ijheatmasstransfer.2004.12.029

Nomenclature

c	particle thermal speed, $c^* = c/(k_B T_{e0}/m_i)^{1/2}$
D	Dawson function, defined in [16]
e	electron charge
F	distribution function
E	electrostatic force
j	current density, $j^* = j/en_{e0}(k_B T_{e0}/m_i)^{1/2}$
k_B	Boltzmann constant
m	particle mass
M	ion-to-electron mass ratio $\equiv m_i/m_e$
M_f	momentum flux, $M_f^* = M_f/n_{e0}k_B T_{e0}$
n	particle density, $n^* = n/n_{e0}$
p	mean pressure, $p^* = p/n_{e0}k_B T_{e0}$
T	temperature
u	fluid velocity, $u^* = u/(k_B T_{e0}/m_i)^{1/2}$
x	Cartesian coordinate
Z_i	ion charge number

Greek symbols

κ	electron-to-ion source temperature ratio at presheath edge $\equiv T_{e0}/T_{i0}$
ρ	reflectivity
Ξ	functions, defined in [16]
τ	fluid-like viscous stress, $\tau^* = \tau/n_{e0}k_B T_{e0}$
ϕ, χ	dimensional and dimensionless potential, $\chi = -e\phi/k_B T_{e0}$
Ω_1, Ω_2	functions, defined in [16]

Superscript

*	dimensionless quantity

Subscripts

b	sheath edge, namely, boundary between sheath and presheath
e, i	electron and ion
tot	total
w	wall
0	presheath edge, namely, coordinate origin at $\phi = 0$ as shown in Fig. 1

several Debye lengths in front of the wall. The electrons are repelled and the ions are accelerated by the negative wall potential. The potential barrier then adjusts itself so that the fluxes of the ions and electrons are equal to the required zero or biased current density through the wall. An ionization region (or presheath) supplies the ions lost to the wall. Small electrostatic potential in the presheath accelerates the ions up to and beyond sonic speed before entering the sheath, as first explicitly pointed out by Bohm [2]. It is important to combine sheath and presheath regions to determine the total momentum flux, ion and electron momentum fluxes incident on the workpiece surface.

In view of the importance of the processes, several plasma-based techniques may be employed to control momentum fluxes of the ions and electrons. For example, an application of a direct current (DC) bias or radio frequency (RF) bias can be used to accelerate the ions and retard the electrons from the plasma to the workpiece surface [3–5]. The sheath acts as a momentum flux filter for the electrons, and transducers that convert electron energy to ion momentum. Since only the very energetic electrons in the distribution can escape from the plasma to the surface, the electron momentum flux to the wall is lower than that which would be if no sheath were present. The ions accelerated by the sheath voltage drop strike the workpiece surface with greater momentum flux than would occur in the absence of a sheath. Therefore, the effects of sheath and net current on the plasma, ion and electron momentum fluxes are of interest.

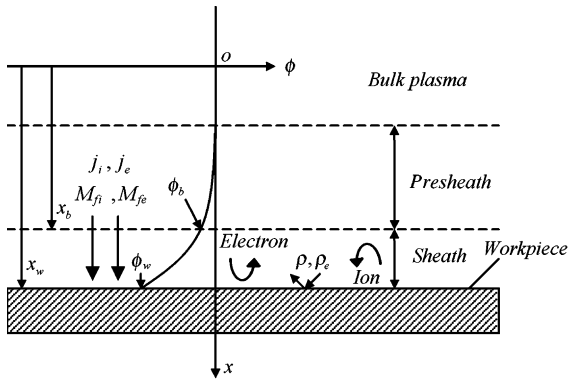

Fig. 1. System sketch for the model and coordinates.

A thin film of liquid metal is often used to withstand the momentum flux carried by the energetic plasma exhaust flow to eliminate erosion, radiation and thermal stress damage in a typical design of a solid divertor. Momentum flux transfer from the plasma to the surface of the liquid metal is responsible for the instabilities and deformation of the free surface. In fusion reactor divertor operation, whether small particles enter the plasma or be reflected away can be determined from the momentum flux exerted on them. Morley et al. [6] applied the fluid code RIPPLE to predict the effect of the momentum flux on the flow of a liquid metal film by introducing momentum influx from the presheath as boundary conditions. Owing to the greater density, Ga

film withstands the momentum flux much better than Li film. Many studies also involve the momentum transfer to target from laser-produced plasmas [7–9]. Glew et al. [10] investigated the properties of plasma-deposited diamond-like carbon films which were dependent of the momentum and energy of the ions. The results showed that the maximum film density and hardness are determined by the maximum film stress at average ion energies of approximately 160 eV. The ion momentum flux increased monotonically with the transmitted power at a fixed pressure.

Collision processes such as charge exchange limit the calculation accuracy of the momentum flux or pressure onto the solid surface from the particle and energy flux data measured by electrostatic probes. Instruments to measure momentum flux from plasma to a workpiece surface have been developed in the past decade [11–13]. Cohen et al. [11] developed a plasma momentum meter to measure momentum flux or total pressure from intense plasma streams of He, Ne, Ar and Kr in a magnetized linear plasma device to a flat carbon target oriented normal to the magnetic field. The results showed that the momentum flux from plasma to target surface increases with increasing negative electrically bias voltage for these four kinds of plasma. In a subsequent publication, Zonca et al. [12] estimated the ion energy from the above experimental data of momentum flux and compared with the prediction by fluid sheath theory. Chavers and Chang-Díaz [13] developed an instrument, a force sensor, used a target plate that immersed in the plasma to measure the momentum flux of plasma and neutral particle jets from magnetized plasmas of H_2, D_2, He and Ar to a flat titanium target. As the ionic and neutral particles with kinetic energies on the order of a few eV impacting the target surface, the measured forces on the surface is 10^{-4} N.

A determination of plasma momentum flux to a workpiece as a function of working parameters controlling the plasma characteristics is still incomplete. A self-consistent and exact determination of the total momentum flux from a kinetic analysis therefore is required. This leads to application of a rather complete kinetic analyses proposed by Emmert et al. [14] and Wei et al. [15,16] to predict momentum fluxes. The former treated a wall completely absorbing the electrons and ions, while the latter allowed the wall partially reflecting (or secondly emitting) ions and electrons.

This study is to analytically and systematically determine momentum flux transport from a plasma to a biased workpiece surface, which partially reflects or secondly emits ions and electrons. Reflections of ions and electrons are commonly encountered in sputter etching and deposition, ion implantation, and an analytical technique known as ion scattering spectroscopy [17]. The ions and electrons are of more realistic highly non-Maxwell–Boltzmann velocity distributions [15,16]. Accounting for the external biased voltage, the total ion and electron momentum fluxes and their components at the wall and sheath edge are determined. The present work gives insight into the manifestations of the sheath behavior and net current affecting the plasma, ion and electron momentum fluxes to workpiece surfaces.

2. Kinetic model and analysis

A plasma in contact with an electrically biased or floating surface partially reflecting and secondly emitting ions and electrons is composed of the presheath and sheath, as illustrated in Fig. 1. In view of charge neutrality, electrical potential in the bulk plasma and presheath edge is considered to be zero. The ions in the positive x-direction are accelerated due to negative potential on the surface. On the other hand, the electrons in the forward direction need to overcome potential. The major assumptions made are as follows:

1. The workpiece surface is negative electrically biased.
2. The model is one-dimensional in a thin thickness of the region considered. The plasma is in a quasi-steady state. Velocities of the ions and electrons in the transverse y- and z-directions obey Maxwell–Boltzmann distributions.
3. Transport processes in the plasma near the surface can be modeled as those in the plasma between two parallel plates.
4. Magnetic field is negligible or the direction of magnetic field is parallel to the ion flow. In other words, Larmor radius is greater than the thickness of the presheath. The one-dimensional ion flow therefore can be assured.
5. Collisionless presheath and sheath, the ionization rate is determined from the Emmert et al.'s model [14]. This model is based on the fact that the ions would be a Maxwell-Boltzmann distribution in the absence of an electrostatic field far from the wall. This proposition has been confirmed by measurements of the ion distribution functions from Bachet et al. [18], and a successful comparison between the measured ion density and velocity from Goeckner et al. [19] and Yeh and Wei [5]. Collisionality in the presheath, unfortunately, is often marginal. That is, the mean-free path between ions and electrons is of the same magnitude as the thickness of the presheath. Modeling different kinds of atomic or molecular collisions is complicated and inaccurate. A further study is essentially required.
6. Thermionic and field emissions of ions and electrons are ignored.

7. The effects of neutral particles are ignored.
8. Ion and electron reflectivities are constant. The secondary emissions of ions and electrons can be included into the reflectivities [20].

2.1. Transport variables in sheath

The transport variables including dimensionless ion density, fluid velocity, mean pressure, and fluid-like shear stress at the sheath edge can be, respectively, derived from different moments of an ion distribution function [16]

$$n^*_{ib} = \frac{1}{Z_i} e^{-\chi_b} \tag{1}$$

$$u^*_{ib} = \Omega_{1b} \tag{2}$$

$$p^*_{ib} = \frac{n^*_{ib}}{3\kappa}(\Omega_{2b} - \kappa u^{*^2}_{ib} + 2) \tag{3}$$

$$\tau^*_{ib} = 2\left(\frac{n^*_{ib}}{\kappa} - p^*_{ib}\right) \tag{4}$$

where the functions Ω_{1b} and Ω_{2b} in Eqs. (2) and (3) are, respectively, defined in [16]. The dimensionless sheath edge potential in Eq. (1) is satisfied by

$$\frac{2}{\sqrt{\pi Z_i \kappa}} D\left(\sqrt{\chi_b}\right) = e^{Z_i \kappa \chi_b} \operatorname{erfc}\left(\sqrt{Z_i \kappa \chi_b}\right) \tag{5}$$

Dawson and the complementary error functions, $D(\sqrt{x})$ and $\operatorname{erfc}(\sqrt{x})$, in Eq. (5) are defined in [16]. The corresponding dimensionless transport variables of the ions and electrons in the sheath are, respectively [16]

$$n^*_i = \frac{1}{Z_i}\left\{\Xi_2(\chi) + e^{Z_i \kappa \chi} \operatorname{erfc}\left[\sqrt{Z_i \kappa(\chi - \chi_b)}\right] - \Xi_1(\chi)\right\} \tag{6}$$

$$u^*_i = \frac{1}{n^*_i Z_i} e^{-\chi_b} \Omega_{1b} \tag{7}$$

$$p^*_i = \frac{1}{3}\left(\Xi_3(\chi) - n^*_i u^{*^2}_i + \frac{2}{\kappa} n^*_i\right) \tag{8}$$

$$\tau^*_i = n^*_i u^{*^2}_i + p^*_i - Z_i E^*_i - n^*_{ib} u^{*^2}_{ib} - p^*_{ib} + \tau^*_{ib} \tag{9}$$

$$n^*_e = e^{-\chi}\left[1 + \frac{\rho_e - 1}{2} \operatorname{erfc}\left(\sqrt{\chi_w - \chi}\right)\right] \tag{10}$$

$$u^*_e = \frac{(1-\rho_e)}{n^*_e}\sqrt{\frac{M}{2\pi}} e^{-\chi_w} \tag{11}$$

$$p^*_e = \frac{1}{3}\left(\Xi_4(\chi) - \frac{1}{M} n^*_e u^{*^2}_e + 2n^*_e\right) \tag{12}$$

$$\tau^*_e = \frac{n^*_e u^{*^2}_e}{M} + p^*_e + E^*_e - \frac{n^*_{eb} u^{*^2}_{eb}}{M} - p^*_{eb} + \tau^*_{eb} \tag{13}$$

where dimensionless functions $\Xi_1(\chi)$, $\Xi_2(\chi)$, $\Xi_3(\chi)$, $\Xi_4(\chi)$ and electrical field intensity acting on the ions E^*_i are defined in [16]. Dimensionless electric field intensity acting on the electrons in Eq. (13) is given by

$$E^*_e \equiv \int_{\chi_b}^{\chi} n^*_e \, d\chi' = \Xi_{4b}(\chi_b) - \Xi_4(\chi) \tag{14}$$

The dimensionless net current density at the wall is given by

$$j^* = j^*_{iw} - j^*_{ew} \tag{15}$$

where the ion and electron current densities at the wall are, respectively,

$$j^*_{iw} = Z_i n^*_{iw} u^*_{iw} = Z_i n^*_{ib} u^*_{ib}, \quad j^*_{ew} = n^*_{ew} u^*_{ew} \tag{16}$$

Eq. (15) is the coupling relationship between the electrons and ions. The dimensionless wall potential is determined by substituting Eqs. (16), (6), (7), (10) and (11) into Eq. (15)

$$\chi_w = \ln\left(\frac{1-\rho_e}{j^*_{iw} - j^*}\sqrt{\frac{M}{2\pi}}\right) \tag{17}$$

When net current density $j^* = 0$, the wall is electrically floating, while the externally biased effect is strong for $j^* \to j^*_{iw}$.

2.2. Momentum flux transport to a biased surface

The dimensional total momentum flux of the ions at a location is given by [21]

$$M_{fi} = \int_{-\infty}^{\infty} F_i m_i c_x^2 \, dc_x \tag{18}$$

where F_i is the ion distribution function [16]. Integrating Eq. (18) by introducing the ion distribution function, dimensionless ion momentum flux in the sheath can be expressed in terms of fluid-like components

$$M^*_{fi} = n^*_i u^{*^2}_i + p^*_i - \tau^*_i \tag{19}$$

where terms on the right-hand side represent fluid inertia, mean pressure, and fluid-like viscous stress of the ions, respectively. Substituting Eq. (1) through Eq. (4) into Eq. (19), dimensionless momentum flux of the ions at the sheath edge is found to be

$$M^*_{fib} = n^*_{ib} u^{*^2}_{ib} + p^*_{ib} - \tau^*_{ib} = \frac{n^*_{ib}\Omega_{2b}}{\kappa} \tag{20}$$

Combining Eqs. (9), (19) and (20), the dimensionless total ion momentum flux at the wall leads to

$$M^*_{fiw} = n^*_{iw} u^{*^2}_{iw} + p^*_{iw} - \tau^*_{iw} = M^*_{fib} + Z_i E^*_{iw} \tag{21}$$

where the last term on the right-hand side represents the momentum flux due to electrical force. In view of electrostatic force, ion momentum flux at the wall is greater than that at the sheath edge. Similarly, the electron momentum flux at a location is given by [21]

$$M_{\mathrm{fe}} = \int_{-\infty}^{\infty} F_{\mathrm{e}} m_{\mathrm{e}} c_x^2 \, \mathrm{d}c_x \tag{22}$$

where F_{e} is the electron distribution function [16]. Substituting the electron distribution function and integrating Eq. (22), dimensionless electron momentum flux in the sheath is found to be

$$M_{\mathrm{fe}}^* = \frac{n_{\mathrm{e}}^* u_{\mathrm{e}}^{*2}}{M} + p_{\mathrm{e}}^* - \tau_{\mathrm{e}}^* = \Xi_4(\chi) \tag{23}$$

Substituting Eq. (13) into Eq. (23), the dimensionless electron momentum flux at the wall is given by

$$M_{\mathrm{few}}^* = \frac{n_{\mathrm{ew}}^* u_{\mathrm{ew}}^{*2}}{M} + p_{\mathrm{ew}}^* - \tau_{\mathrm{ew}}^* = M_{\mathrm{feb}}^* - E_{\mathrm{ew}}^* \tag{24}$$

where dimensionless electron momentum flux at the sheath edge is

$$M_{\mathrm{feb}}^* = \frac{n_{\mathrm{eb}}^* u_{\mathrm{eb}}^{*2}}{M} + p_{\mathrm{eb}}^* - \tau_{\mathrm{eb}}^* = \Xi_{4\mathrm{b}}(\chi_{\mathrm{b}}) \tag{25}$$

Substituting Eq. (10) through Eq. (13) into Eq. (23), the dimensionless momentum flux of the electrons at the wall further becomes

$$M_{\mathrm{few}}^* = \Xi_{4\mathrm{w}}(\chi_{\mathrm{w}}) = n_{\mathrm{ew}}^* = \frac{\rho_{\mathrm{e}} + 1}{2} \mathrm{e}^{-\chi_{\mathrm{w}}} \tag{26}$$

which shows that an increase of wall potential reduces electron momentum flux at the wall. Furthermore, dimensionless electron momentum flux is identical to dimensionless electron density at the wall. Combining Eqs. (20) and (25), the total momentum flux, including that of the ions and electrons, at the sheath edge is found to be

$$\begin{aligned} M_{\mathrm{f\,tot\,b}}^* &= M_{\mathrm{fib}}^* + M_{\mathrm{feb}}^* \\ &= \frac{n_{\mathrm{ib}}^* \Omega_{2\mathrm{b}}}{\kappa} + \mathrm{e}^{-\chi_{\mathrm{b}}} + \frac{\rho_{\mathrm{e}} - 1}{2} \\ &\quad \times \left[\mathrm{e}^{-\chi_{\mathrm{b}}} \operatorname{erfc}\left(\sqrt{\chi_{\mathrm{w}} - \chi_{\mathrm{b}}}\right) + 2\sqrt{\frac{\chi_{\mathrm{w}} - \chi_{\mathrm{b}}}{\pi}} \mathrm{e}^{-\chi_{\mathrm{w}}} \right] \end{aligned} \tag{27}$$

Combining Eqs. (20), (21) and (26), the dimensionless total momentum flux on the biased wall yields

$$\begin{aligned} M_{\mathrm{f\,tot\,w}}^* &= M_{\mathrm{fiw}}^* + M_{\mathrm{few}}^* \\ &= \frac{n_{\mathrm{ib}}^* \Omega_{2\mathrm{b}}}{\kappa} + Z_{\mathrm{i}} E_{\mathrm{iw}}^* + \frac{\rho_{\mathrm{e}} + 1}{2} \mathrm{e}^{-\chi_{\mathrm{w}}} \end{aligned} \tag{28}$$

The error, Dawson, and incomplete gamma functions were numerically integrated by a Simpson's rule. Relative errors were less than 10^{-6} by comparing grids of 1000 and 500.

3. Results and discussion

In this study, dimensionless independent parameters controlling momentum transport from the plasma including the presheath and sheath to a workpiece surface are ion reflectivity (ρ) and electron reflectivity (ρ_{e}) of the wall, ion-to-electron mass ratio (M), charge number (Z_{i}), the electron-to-ion source temperature at the presheath edge (κ), and net current density (j^*).

To confirm relevancy and accuracy of this model, the predicted total momentum flux at the wall between a helium plasma and carbon workpiece as a function of negative electrically biased voltage in this work is compared with experimental data provided by Cohen et al. [11], as shown in Fig. 2. Choosing dimensionless parameters $Z_{\mathrm{i}} = 1$, $\rho = 0.5$, $\rho_{\mathrm{e}} = 0.5$, $M = 7344$, $\kappa = 1$, and $n_{\mathrm{e0}} = 2.0 \times 10^{19}\ \mathrm{m}^{-3}$, $m_{\mathrm{i}} = 6.68 \times 10^{-27}\ \mathrm{kg}$, $T_{\mathrm{e0}} = 1.0 \times 10^5\ \mathrm{K}$, the predicted total momentum flux at the wall as a function of negative electrically biased voltage agrees quite well with experimental data. Good comparisons between the predicted and measured ion density and velocity as a function of wall potential in the sheath can be seen in [5].

Spatial variations of dimensionless ion momentum flux and its components, including fluid inertia, mean pressure, and fluid-like viscous stress, in the sheath with dimensionless potential for different ion reflectivities and dimensionless net current densities are shown in Fig. 3. Dimensionless potential of 0.404 is referred to the sheath edge, while 2.965, 3.804, and 4.064 are potentials at the wall, respectively, for $\rho = 0$, $j^* = 0$, $\rho = 0$, $j^* = 0.5$, and $\rho = 0.5$, $j^* = 0$. Dimensionless wall potential is increased to reduce electron current density as ion reflectivity and net current density increase (see Eq. (17)). Except for

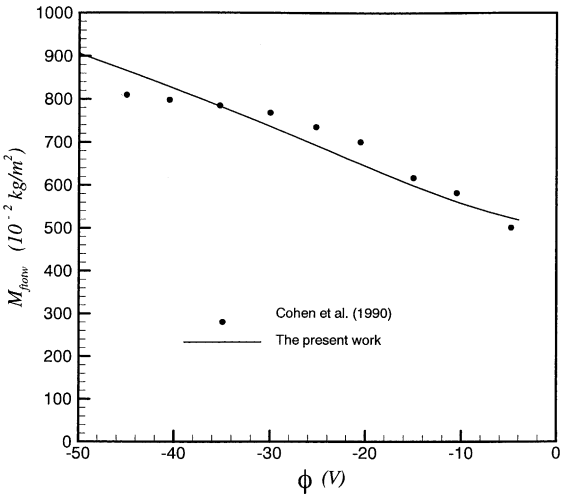

Fig. 2. A comparison between the predicted total momentum flux as a function of negative electrically biased voltage at wall and experimental result [11].

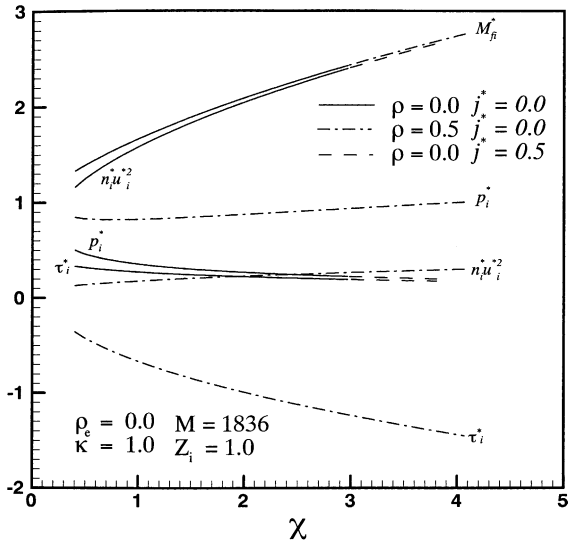

Fig. 3. Spatial variations of dimensionless total ion momentum (M_{fi}^*), fluid inertia ($n_i^* u_i^{*2}$), mean pressure (p_i^*), and fluid-like viscous stress (τ_i^*) in sheath for different ion reflectivities (ρ) and net current densities (j^*).

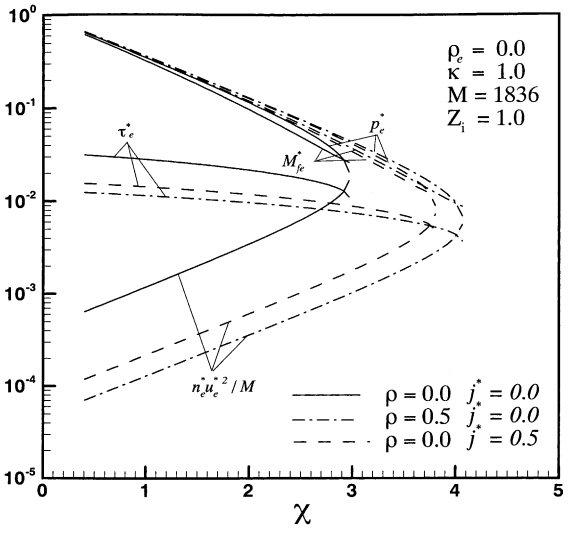

Fig. 4. Spatial variations of dimensionless total electron momentum (M_{fe}^*), fluid inertia ($n_e^* u_e^{*2}/M$), mean pressure (p_e^*), and fluid-like viscous stress (τ_e^*) in sheath for different ion reflectivities (ρ) and net current densities (j^*).

wall potential, the variations in ion momentum flux and its components with potential are independent of net current density. Ion momentum flux and fluid inertia always increase monotonically in the forward direction due to the action of electrostatic field. Mean pressure at the wall decrease with increasing net current density and decreasing ion reflectivity. The former is a result of the increase in dimensionless wall potential. Fluid-like viscous stress acts as a driving force for zero ion reflectivity and a retarding force for ion reflectivity of 0.5 [16]. Fluid-like viscous stress accounting for the direction at the wall is decreased with increasing net current and ion reflectivity. The ion momentum flux is dominated by fluid inertia.

Similar dimensionless momentum fluxes of the electrons across the sheath for different ion reflectivities and dimensionless net current densities are presented in Fig. 4. Except for fluid inertia, dimensionless momentum flux, mean pressure and fluid-like viscous stress of the electrons decrease in the forward direction. In contrast to the ions, fluid-like viscous stress of the electrons is a driving force in all cases. Momentum flux and mean pressure of the electrons increase, fluid inertia and fluid-like viscous stress decrease with increasing net current and ion reflectivity. The major and minor contributions of the electron momentum flux are mean pressure and fluid inertia, respectively. The components of electron momentum flux become the same order of magnitude as the wall is approached.

The effects of dimensionless net current density on the dimensionless ion momentum flux and its components at the sheath edge and wall are, respectively, shown in Fig. 5. In view of the ions driven by electrostatic field, the ion momentum flux and fluid inertia at the wall are higher than those at the sheath edge. Mean pressure and fluid-like viscous stress at the wall, however, are lower than those at the sheath edge. In contrast to being constants at the sheath edge, ion momentum

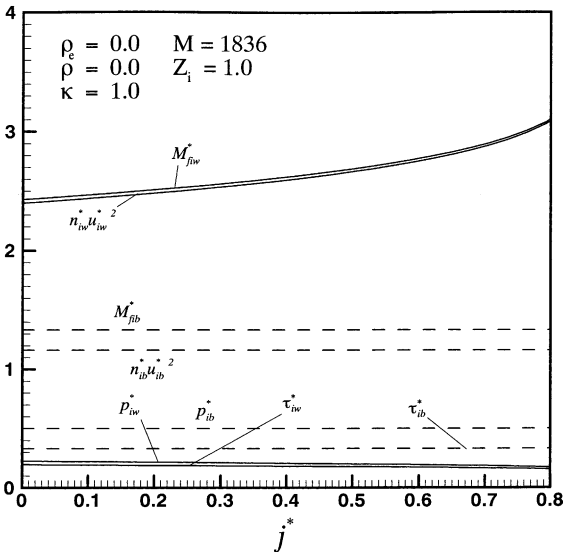

Fig. 5. Dimensionless total ion momentum fluxes (M_{fib}^*, M_{fiw}^*), fluid inertia ($n_{ib}^* u_{ib}^{*2}$, $n_{iw}^* u_{iw}^{*2}$), mean pressures (p_{ib}^*, p_{iw}^*), and fluid-like viscous stresses (τ_{ib}^*, τ_{iw}^*) at sheath edge and wall versus net current density (j^*).

flux and fluid inertia increase, mean pressure and fluid-like viscous stress decrease at the wall with increasing net current density. As dimensionless net current density is 0 and 0.8, the corresponding dimensionless ion momentum flux at the wall is around 2.43 and 3.12, respectively. Since the ion momentum flux at the sheath edge is 1.33, the ratios of the ion momentum flux at the wall to that at the sheath edge are 1.83 and 2.35, respectively. In the absence of the sheath, the ion momentum flux is underestimated seriously for a high net current density.

Similarly, dimensionless momentum fluxes and their components of the electrons at the sheath edge and wall as a function of dimensionless net current density are presented in Fig. 6. Except for momentum flux and mean pressure of the electrons at the sheath edge, fluid inertia and fluid-like viscous stress at the sheath edge, and momentum flux and the components at the wall decrease with increasing net current density. In contrast to fluid inertia, momentum flux, mean pressure, fluid-like viscous stress of the electrons at the wall are lower than those at the sheath edge, as a result of the action of electrostatic field. As dimensionless net current density is 0 and 0.8, the corresponding ratios of the electron momentum flux at the sheath edge to that at the wall are 23.46 and 275, respectively. Without the sheath, the electron momentum flux thus is seriously overestimated for a high net current density.

The variations in dimensionless potentials, total momentum fluxes, and momentum fluxes, current densities and electrostatic forces of the ions and electrons at the wall and sheath edge with ion reflectivity of a floating wall are shown in Fig. 7. Since dimensionless wall potential increases while sheath edge potential remains constant [16], the effects of the sheath become pronounced with increasing ion reflectivity. In contrast to the electrons lost momentum, momentum gained from electrical field for the ions at the wall is increased with increasing ion reflectivity. Current density at the wall decreases with increasing ion reflectivity. This is attributed to reduction of ion speed or current density at the sheath edge and conservation of current density through the sheath [16]. In view of electrostatic force, ion and electron momentum fluxes at the sheath edge are, respectively, lower and higher than that at the wall. Momentum fluxes of the ions at the sheath edge and wall are greater than those of the electrons for different ion reflectivities. For ion reflectivity of 0 and 0.9 the corresponding ion-to-electron momentum flux ratio at the wall is around 93 and 2314, respectively. The ion-to-electron momentum flux ratio at the wall therefore increases significantly with ion reflectivity. The ratio of the total momentum flux at the wall to that at the sheath edge is greater than unity and increases with ion reflectivity.

The effects of electron reflectivity on the total and components of dimensionless ion and electron momentum fluxes at the sheath edge and wall are presented in Fig. 8. An increase in electron reflectivity reduces dimensionless wall potential, while sheath edge potential remains constant. Increasing electron reflectivity indicates a reduction of electron current density, which results in a decrease of ion current by reducing

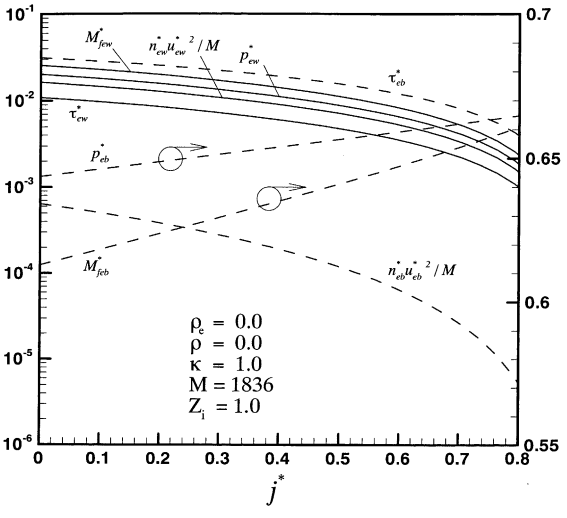

Fig. 6. Dimensionless total electron momentum fluxes (M^*_{feb}, M^*_{few}), fluid inertia ($n^*_{eb}u^{*2}_{eb}/M$, $n^*_{ew}u^{*2}_{ew}/M$), mean pressures (p^*_{eb}, p^*_{ew}), and fluid-like viscous stresses (τ^*_{eb}, τ^*_{ew}) at sheath edge and wall versus net current density (j^*).

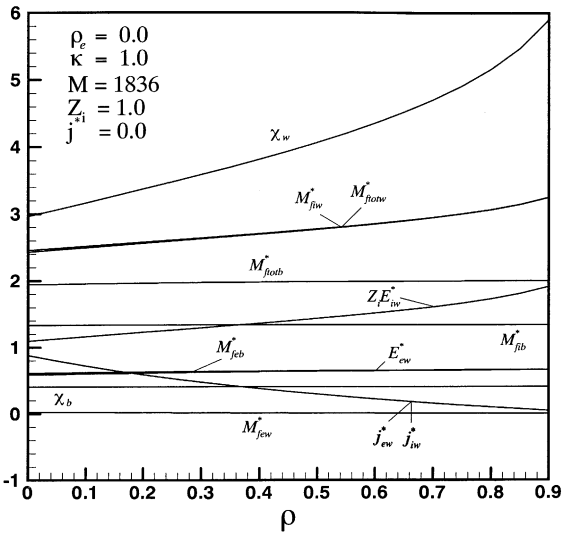

Fig. 7. Dimensionless sheath edge and wall potentials (χ_b, χ_w), ion and electron momentum fluxes (M^*_{fib}, M^*_{feb}, M^*_{fiw}, M^*_{few}) and total momentum fluxes ($M^*_{f\,tot\,b}$, $M^*_{f\,tot\,w}$) at sheath edge and wall, ion and electron current densities (j^*_{iw}, j^*_{ew}) and electrostatic forces ($Z_iE^*_{iw}$, E^*_{ew}) at wall versus ion reflectivity (ρ).

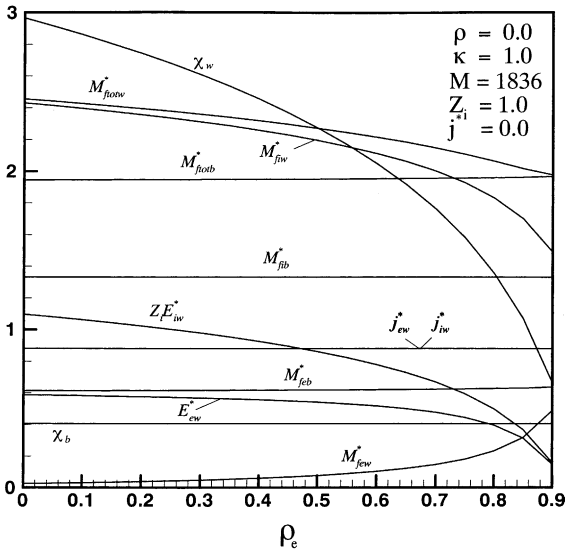

Fig. 8. Dimensionless sheath edge and wall potentials (χ_b, χ_w), ion and electron momentum fluxes (M^*_{fib}, M^*_{feb}, M^*_{fiw}, M^*_{few}) and total momentum fluxes ($M^*_{f\,tot\,b}$, $M^*_{f\,tot\,w}$) at sheath edge and wall, ion and electron current densities (j^*_{iw}, j^*_{ew}) and electrostatic forces ($Z_iE^*_{iw}$, E^*_{ew}) at wall versus electron reflectivity (ρ_e).

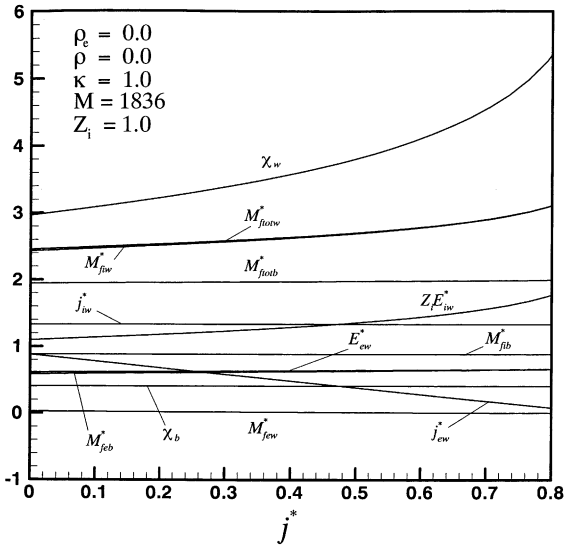

Fig. 9. Dimensionless sheath edge and wall potentials (χ_b, χ_w), ion and electron momentum fluxes (M^*_{fib}, M^*_{feb}, M^*_{fiw}, M^*_{few}) and total momentum fluxes ($M^*_{f\,tot\,b}$, $M^*_{f\,tot\,w}$) at sheath edge and wall, ion and electron current densities (j^*_{iw}, j^*_{ew}) and electrostatic forces ($Z_iE^*_{iw}$, E^*_{ew}) at wall versus net current density (j^*).

dimensionless wall potential. It can also be seen that ion momentum flux and its components at the sheath edge are independent of electron reflectivity. Dimensionless ion and electron momentum fluxes at the wall decrease and increase with increasing electron reflectivity, respectively. This is attributed to a decrease in electric field with increasing electron reflectivity. Electron momentum flux at the wall thus cannot be neglected for a high electron reflectivity. Since ion and electron momentum fluxes at the wall, respectively, approach that at the sheath edge, the effects of the sheath on ion and electron momentum fluxes can be neglected for a high electron reflectivity. The decrease in the total momentum flux at the wall with increasing electron reflectivity is a result of a reduction of ion momentum flux.

Dimensionless potentials, ion and electron momentum fluxes at the wall and sheath edge, and current densities at the wall versus net current density are presented in Fig. 9. In view of constant sheath edge potential, dimensionless wall potential increases with net current density. The effects of the sheath therefore are important for a high net current density. An increase in net current density results in a decrease in electron current density at the wall. This is because ion current density in the sheath is determined by that at the sheath edge, which is independent of net current density. Ion momentum flux at the sheath edge is independent of net current density. In view of electrostatic force, ion momentum flux at the wall is greater than that at the sheath edge, in contrast to electron momentum flux at the wall. Irrespective of net current density, ion momentums at the wall and sheath edge are larger than those of the electrons. As dimensionless net current density is 0 and 0.8, the corresponding ion-to-electron momentum flux ratio at the wall is about 93 and 1155, respectively. The contribution of electron momentum flux to the total momentum flux at the wall, therefore, can be ignored with high net current density. Since dimensionless wall potential, ion and electron electrostatic forces increase with net current density, contribution of ion electrostatic force to the total momentum flux at the wall is increased with net current. The total momentum fluxes at the wall and sheath edge increase with net current. Provided that the sheath is ignored, the total momentum flux at the wall is seriously underestimated for a high net current density.

The effects of the electron-to-ion source temperature ratio at the presheath edge on dimensionless potentials, electrical forces and momentum fluxes of the ions and electrons at the sheath edge and wall are shown in Fig. 10. It can be seen that dimensionless sheath edge and wall potentials increase with increasing the electron-to-ion source temperature ratio at the presheath edge. An increase in the electron-to-ion source temperature ratio at the presheath edge indicates ionization rate is small [14,15]. Current density therefore is decreased with increasing the electron-to-ion source temperature ratio at the presheath edge. Dimensionless electron and ion momentum fluxes and total momentum fluxes at the sheath edge and wall, electrical forces at the wall decrease with increasing electron-to-ion source tempera-

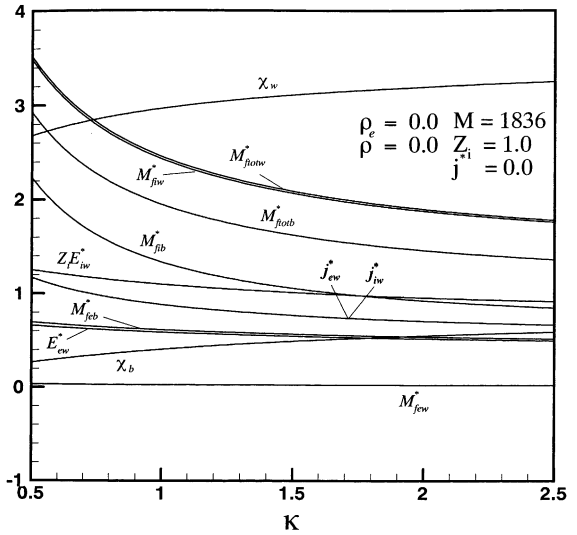

Fig. 10. Dimensionless sheath edge and wall potentials (χ_b, χ_w), ion and electron momentum fluxes (M^*_{fib}, M^*_{feb}, M^*_{fiw}, M^*_{few}) and total momentum fluxes ($M^*_{f\,tot\,b}$, $M^*_{f\,tot\,w}$) at sheath edge and wall, ion and electron current densities (j^*_{iw}, j^*_{ew}) and electrostatic forces ($Z_iE^*_{iw}$, E^*_{ew}) at wall versus electron-to-ion source temperature ratio at presheath edge (κ).

ture ratio at the presheath edge. As the electron-to-ion source temperature ratio at the presheath edge increases, the ion-to-electron momentum flux ratio at the wall decreases and indicates importance of electron momentum flux at the wall.

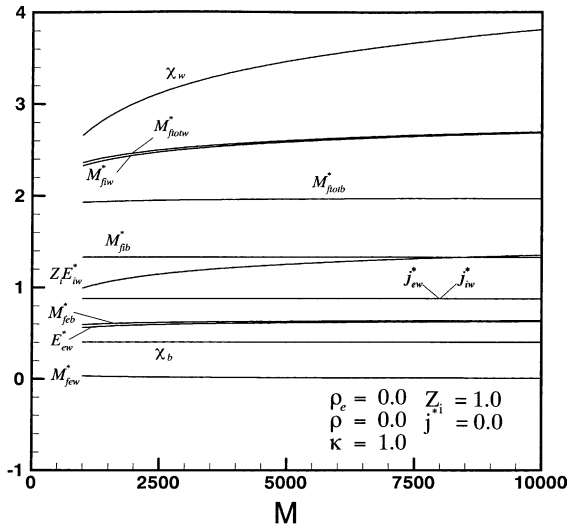

Fig. 11. Dimensionless sheath edge and wall potentials (χ_b, χ_w), ion and electron momentum fluxes (M^*_{fib}, M^*_{feb}, M^*_{fiw}, M^*_{few}) and total momentum fluxes ($M^*_{f\,tot\,b}$, $M^*_{f\,tot\,w}$) at sheath edge and wall, ion and electron current densities (j^*_{iw}, j^*_{ew}) and electrostatic forces ($Z_iE^*_{iw}$, E^*_{ew}) at wall versus ion-to-electron mass ratio (M).

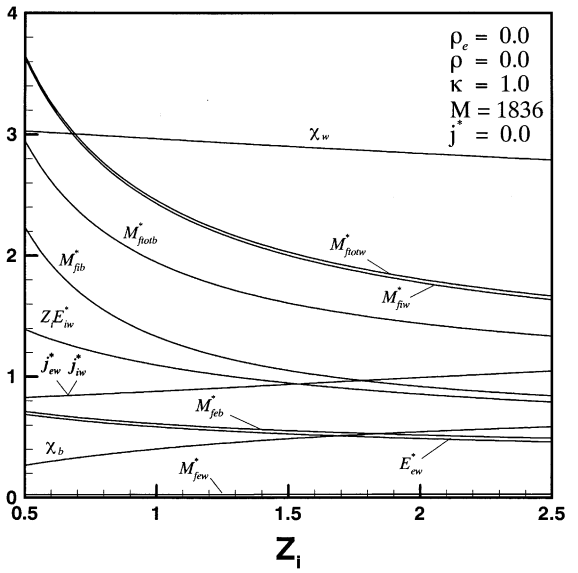

Fig. 12. Dimensionless sheath edge and wall potentials (χ_b, χ_w), ion and electron momentum fluxes (M^*_{fib}, M^*_{feb}, M^*_{fiw}, M^*_{few}) and total momentum fluxes ($M^*_{f\,tot\,b}$, $M^*_{f\,tot\,w}$) at sheath edge and wall, ion and electron current densities (j^*_{iw}, j^*_{ew}) and electrostatic forces ($Z_iE^*_{iw}$, E^*_{ew}) at wall versus charge number (Z_i).

Dimensionless ion and electron momentum fluxes, potentials at the sheath edge and wall, electrical forces at the wall versus the ion-to-electron mass ratio are shown in Fig. 11. Dimensionless sheath edge potential, ion and electron current densities, ion momentum flux at the sheath edge are independent of the ion-to-electron mass ratio. Except for electron momentum flux at the wall, total momentum flux, ion moment flux, momentum fluxes due to electrical field and ion-to-electron momentum flux ratio at the wall increase with increasing the ion-to-electron mass ratio. The effects of charge number on dimensionless total momentum flux, ion and electron momentum fluxes, potentials at the wall and sheath, and current densities are presented in Fig. 12. Dimensionless sheath edge potential, ion and electron current densities at the wall increase with charge number. Aside from a slight increase of electron momentum flux at the wall, dimensionless total momentum flux and ion momentum fluxes at the sheath edge and wall, and potential and electrical forces at the wall decrease with increasing charge number.

4. Conclusions

The conclusions drawn are the following:

1. The total momentum flux, ion and electron momentum fluxes at the wall and sheath edge, ion and

electron current densities and electrostatic forces at the wall affected by dimensionless parameters are summarized as follows:

(a) Increasing net current density, ion reflectivity, ion-to-electron mass ratio, and decreasing the electron-to-ion source temperature ratio at the presheath edge and charge number enhance the total momentum flux at the sheath edge and wall, and ion momentum flux at the wall. An increase of electron reflectivity results in a decrease of the total and ion momentum fluxes at the wall and increase of the total momentum flux at the sheath edge. Ion momentum flux at the sheath edge is independent of ion and electron reflectivity, ion-to-electron mass ratio, and net current density, while it increases with decreases of the electron-to-ion source temperature ratio at the presheath edge and charge number.

(b) Decreasing ion reflectivity, electron-to-ion source temperature ratio at the presheath edge, ion-to-electron mass ratio and net current density, and increasing electron reflectivity and charge number increase electron momentum flux at the wall. In contrast to the wall, electron momentum flux at the sheath edge increases with increasing ion and electron reflectivities, ion-to-electron mass ratio and net current density, and decreasing the electron-to-ion source temperature ratio at the presheath edge and charge number.

(c) Increasing ion reflectivity, ion-to-electron mass ratio and net current density, and decreasing electron reflectivity, electron-to-ion source temperature ratio at the presheath edge and charge number increase ion and electron electrostatic forces at the wall.

(d) Decreases in ion reflectivity, electron-to-ion source temperature ratio at the presheath edge, and an increase in charge number enhance ion and electron current densities at the wall. Increasing net current density results in a decrease of electron current density. Ion and electron current densities are independent of electron reflectivity and ion-to-electron mass ratio.

2. Choosing higher ion reflectivity, ion-to-electron mass ratio and net current density, and lower electron reflectivity, electron-to-ion source temperature ratio at the presheath edge and charge number results in an increase of the total momentum flux at the wall.
3. Contribution of electron momentum flux to the total momentum flux at the wall is reduced by increasing net current density, ion reflectivity, ion-to-electron mass ratio, and decreasing electron reflectivity, electron-to-ion source temperature ratio at the presheath edge and charge number.
4. The effects of the sheath on the total momentum flux transport to the wall, ion and electron momentum fluxes at the wall and sheath edge are summarized as follows:

(a) Increasing ion reflectivity, electron-to-ion source temperature ratio at the presheath edge, ion-to-electron mass ratio, charge number, net current density and decreasing electron reflectivity enhance the ratio of the total momentum fluxes between the wall and sheath edge. In the absence of the sheath, underestimated predictions of the total momentum flux at the wall suffer serious errors. The effects of the sheath on predicting the total momentum flux transport to a biased workpiece surface are important.

(b) Increasing ion reflectivity, electron-to-ion source temperature ratio at the presheath edge, ion-to-electron mass ratio, and net current density, and decreasing electron reflectivity increase the ratio of ion momentum fluxes between the wall and sheath edge. The ratio of electron momentum fluxes between the sheath edge and wall is increased with increasing ion reflectivity, electron-to-ion source temperature ratio at the presheath edge, ion-to-electron mass ratio, net current density, and decreasing electron reflectivity. An increase of charge number, however, results in an increase of the ratio of ion momentum fluxes between the wall and sheath edge and a decrease of the ratio of electron momentum fluxes between the sheath edge and wall. Without the sheath, ion and electron momentum fluxes are, respectively, underestimated and overestimated seriously.

References

[1] F.F. Chen, Introduction to Plasma Physics, Plenum Press, New York, 1974.
[2] D. Bohm, Minimum ionic kinetic energy for a stable sheath, in: A. Guthrie, R. Wakerling (Eds.), The Characteristics of Electrical Discharges in Magnetic Fields, McGraw-Hill, New York, 1949, pp. 77–86.
[3] K. Shirai, S. Gonda, Study of the substrate bias in plasma depositions using an electron cyclotron resonance plasma, J. Appl. Phys. 68 (1990) 4258–4267.
[4] F. Thièry, Y. Pauleau, L. Ortega, Effect of the substrate bias voltage on the physical characteristics of cooper films deposited by microwave plasma-assisted sputtering technique, J. Vac. Sci. Technol. A 22 (2004) 30–35.
[5] F.B. Yeh, P.S. Wei, Plasma energy transport to an electrically biased surface, Int. J. Heat Mass Transfer 47 (2004) 4019–4029.
[6] N.B. Morley, A.A. Gaizer, M.A. Abdou, Estimates of the effect of a plasma momentum flux on the free surface of a thin film of liquid metal, Fus. Eng. Des. 28 (1995) 176–180.
[7] D.J. Albares, Electron and ion momentum transfer from plasma electrical conductivity in a magnetic field, Phys. Fluid 16 (1973) 1252–1259.

[8] K. Kuriki, Y. Kitora, Momentum transfer to target from laser-produced plasma, Appl. Phys. Lett. 30 (1977) 443–446.
[9] D.W. Koopman, Momentum transfer interaction of a laser-produced plasma with a low-pressure background, Phys. Fluids 15 (1972) 1959–1969.
[10] A.D. Glew, R. Saha, J.S. Kim, M.A. Cappelli, Ion energy and momentum flux dependence of diamond-like carbon film synthesis in radio frequency discharges, Surf. Coatings Technol. 114 (1999) 224–229.
[11] S.A. Cohen, F. Zonca, J. Timberlake, T. Bennett, J. Cuthbertson, W. Langer, R. Motley, An instrument for measuring the momentum flux from atomic and charged particle jets, Rev. Sci. Instrum. 61 (1990) 3586–3591.
[12] F. Zonca, S.A. Cohen, J. Cuthbertson, J. Timberlake, D. Ruzic, Measurements of plasma flows in a divertor simulation, J. Nucl. Mater. 176 & 177 (1990) 746–749.
[13] D.G. Chavers, F.R. Chang-Díaz, Momentum flux measuring instrument for neutral and charged particle flows, Rev. Sci. Instrum. 73 (2002) 3500–3507.
[14] G.A. Emmert, R.M. Wieland, A.T. Mense, J.N. Davidson, Electric sheath and presheath in a collisionless, finite ion temperature plasma, Phys. Fluids 23 (1980) 803–812.
[15] P.S. Wei, F.B. Yeh, C.Y. Ho, Distribution function of positive ions and electrons in a plasma near a surface, IEEE Trans. Plasma Sci. 28 (2000) 1244–1253.
[16] P.S. Wei, F.B. Yeh, Fluid-like transport variables in a kinetic, collisionless plasma near a surface with ion and electron reflection, IEEE Trans. Plasma Sci. 28 (2000) 1233–1243.
[17] B. Chapman, Glow Discharge Processes, Sputtering and Plasma Etching, Wiley, New York, 1980.
[18] G. Bachet, L. Chérigier, F. Doveil, Ion velocity distribution function observations in a multipolar argon discharge, Phys. Plasmas 2 (1995) 1782–1788.
[19] M.J. Goeckner, J. Goree, T.E. Sheridan, Measurements of ion velocity and density in the plasma sheath, Phys. Fluids B 4 (1992) 1663–1670.
[20] P.C. Stangeby, The plasma sheath, in: D.E. Post, R. Behrisch (Eds.), Physics of Plasma Wall Interactions in Controlled Fusion, Proceedings of NATO Advanced Study Institute, July 30–August 10, 1984, Val-Morin, Quebec, Canada, Plenum, New York, 1986, pp. 41–97.
[21] W.G. Vincenti, C.H. Kruger Jr., Introduction to Physical Gas Dynamics, Wiley, New York, 1970.